DOI: 10.1002/ejic.200900344

The Reasons for Ligand-Dependent Quantum Yields and Absorption Spectrum of Four Polypyridylruthenium(II) Complexes with a Tetrazolate-Based Ligand: TDDFT Study

Xiao-Na Li,[a,b] Zhi-Jian Wu,[a] Hong-Jie Zhang,*[a] Zhen-Jun Si,[a] Liang Zhou,[a,b] and Xiao-Juan Liu[a]

Keywords: Ruthenium / Absorption / N ligands / Density functional calculations

The quantum yield, lifetime, and absorption spectrum of four $[Ru(bpy)_2L]^+$ [where bpy is 2,2′-bipyridyl; L is represented by the deprotonated form of 2-(1*H*-tetrazol-5-yl)pyridine (L1) or 2-(1*H*-tetrazol-5-yl)pyrazine (L2)], as well as their methylated complexes $[Ru(bpy)_2LMe]^{2+}$ (RuL1Me and RuL2Me) are closely ligand dependent. In this paper, density functional theory (DFT) and time-dependent DFT (TDDFT) were performed to compare the above properties among these complexes. The calculated results reveal that the replacement of pyridine by pyrazine or the attachment of a CH_3 group to the tetrazolate ring greatly increases the π-accepting ability of the ancillary ligands. The stronger π-accepting ability of the ancillary ligands in RuL2 results in stronger interaction with polar solvents and a relaxed geometrical structure; these are the main reasons for the lowest quantum yields and the shortest lifetime. The electron-donating CH_3 group buffers the interaction between RuL2Me and the solvent, and together with the enhanced MLCT participation, these account for the highest quantum yields and the longest lifetime. This theoretical contribution allows the factors determining the efficiency of radiative and nonradiative decay pathways in this series of complexes to be rationalized and also allows design of new ruthenium(II) complexes with higher phosphorescence efficiency.

Introduction

Since the luminescent properties of $[Ru(bpy)_3]^{2+}$ (bpy = 2,2′-bipyridine) were first reported by Paris and Brandt,[1] ruthenium(II) polypyridine complexes have become the most extensively investigated complexes in coordination chemistry. These Ru^{II} polypyridine complexes exhibit a combination of properties, for instance, high chemical stability, long-lived excited-state lifetimes, significant metal-to-ligand charge transfer (MLCT) absorption in the visible spectral region, reversible electrochemical behavior, and so on. These properties make them suitable as multielectron-transfer catalysts,[2] molecular devices and machines,[3] phosphorescent dopants in optoelectronic devices such as organic light-emitting diodes (OLEDs), as well as fluorescent materials.[4] Besides these applications, significant interest in these complexes lies in the design and optimization of dye-sensitized solar cells (DSSCs), whereby functionalized Ru^{II} complexes are bound onto a TiO_2 electrode surface.[5] To date, several hundreds of Ru^{II}–polypyridine complexes have been synthesized and their properties can be easily tuned by changing the ligands or substituents.[6,7] For example, one can modify the polypyridine directly by replacing the pyridine with other heterocyclic rings.[8] In contrast, the π* orbital can be extended by introducing appropriate substituents that increase the delocalization of the acceptor ligand of the MLCT excited state and reduce the nonradiative decay.[9] In principle, MLCT character can increase the emitting state, and it is considered a general way to improve the quantum yield and efficiency of phosphorescence. However, upon increasing emission energy, the admixture between the metal and the ligand orbitals is generally decreased such that spin–orbit coupling and intersystem crossing are reduced. This consequently results in a decrease in the emission efficiency as a result of the decrease in radiative decay rates (k_r) or an increase in the nonradiative decay rate (k_{nr}) and, therefore, a decrease in the quantum yield is observed as well.

However, for this series of complexes $[Ru(bpy)_2L]^+$ [where L is represented by the deprotonated form of 2-(1*H*-tetrazol-5-yl)pyridine (L1) or 2-(1*H*-tetrazol-5-yl)pyrazine (L2)], as well as their methylated complexes RuL1Me and RuL2Me,[10] the emission energy, quantum yields, and lifetime of RuL2Me are all much larger than those of RuL2 and RuL1. It is still not very clear how the structures of the ligands influence the phosphorescence efficiency after

[a] State Key Laboratory of Rare Earth Resource Utilization, Changchun Institute of Applied Chemistry, Chinese Academy of Sciences and Graduate School of the Chinese, Changchun 130022, P. R. China
Fax: +86-431-85698041
E-mail: hongjie@ciac.jl.cn
[b] Academy of Sciences, Beijing, P. R. China
Supporting information for this article is available on the WWW under http://dx.doi.org/10.1002/ejic.200900344.

modification. This interesting phenomenon stimulated us to investigate the geometrical structures and optical mechanism of this series of complexes. Therefore, a detailed theoretical investigation of electronic structure and spectra properties was performed by using DFT and time-dependent DFT (TDDFT). The aim of the theoretical work is threefold: (1) To compare the geometrical structural difference of the four complexes with different ancillary ligands. (2) To establish how the electronic structures and absorption spectrum are influenced by changing the structure of the ancillary ligands. (3) To compare the different quantum yields among these complexes. This study will be of great benefit when designing new ruthenium(II) complexes with higher phosphorescence quantum yields.

Computational Details

The geometrical structures of the ground-state are optimized by the DFT[11] method with Becke's LYP (B3LYP) exchange-correlation functional.[12] There are no symmetry constraints on these complexes. With such calculations, TDDFT[13] calculations with the use of the B3LYP exchange functional are performed to obtain both singlet and triplet absorption spectra in acetonitrile solvent. To investigate solvent effects, the singlet absorption spectra of the four complexes in the gas phase were also performed at the same level to the absorption in acetonitrile solvent. The solvent effect was simulated by using the polarizable continuum model (PCM),[14] in which the solvent cavity is seen as a union of interlocking atomic spheres. Recent calculations with the TDDFT method for transition-metal complexes have demonstrated its reliability and gave good assignment compared with experimental spectra.[15]

In the calculations, the quasirelativistic pseudopotentials proposed by Hay and Wadt[16] with 16 valence electrons were employed on Ru, and a "double-ξ" quality basis set LANL2DZ was adopted as the basis set. The selection of appropriate basis set for a given system is very important in ensuring high-quality results. However, the trade-off between accuracy and computational costs has to be weighted, and this becomes increasingly important when dealing with large molecular systems. Therefore, as an example, we optimized the geometry structure of RuL2 in the ground state with two sets of basis sets. LANL2DZ on Ru and 6-31G(d) on all the nonmetallic atoms was used as BS1; LANL2DZ on Ru, 6-31G on C and H, and 6-31G(d) on N was used as BS2. The calculated results are shown in Table 1. As shown, the geometry obtained by BS2 is more consistent with the experimental values compared with that obtained by BS1. The absorption spectra are slightly changed by using different basis sets (BS1 and BS2). Therefore, we adopted BS2 for all the calculations. The frequency calculations were also performed to verify the optimized structure to be at an energy minimum. All the calculations were performed with the Gaussian 03 software package[17] on an Origin/3900 server.

Table 1. Main optimized geometry parameters of the four complexes in the gas phase at the B3LYP/LANL2DZ level (with RuL2 with different basis sets) together with the experimental data of RuL2.

	RuL1	RuL2		RuL1Me	RuL2Me	expt.[10]
	S_0	S_0(BS1)	S_0(BS2)	S_0	S_0	
	Bond length [Å]					
Ru–N1	2.164	2.158	2.153	2.169	2.154	2.040
Ru–N2	2.068	2.068	2.070	2.105	2.111	2.084
Ru–N3	2.097	2.104	2.100	2.113	2.115	2.063
Ru–N4	2.116	2.123	2.116	2.101	2.101	2.055
Ru–N5	2.102	2.107	2.103	2.115	2.100	2.058
Ru–N6	2.093	2.097	2.094	2.098	2.118	2.048
C1–C2	1.447	1.444	1.442	1.455	1.451	1.444
	Angle [°]					
N2–Ru–N4	171.0	171.1	171.1	172.4	172.3	171.46
	Dihedral angle [°]					
N6–N5–Ru–N4	91.4	91.4	88.8	91.5	89.1	97.5
N1–N2–Ru–N5	–96.8	–96.8	–100.7	–97.1	–97.7	98.0

Results and Discussion

Geometries in the Ground State

The sketch structures of the four complexes are shown in Scheme 1, and the optimized ground-state geometrical structures of RuL2 and RuL2Me are shown in Figure 1 along with the numbering of some key atoms. The main geometry structural parameters are summarized in Table 1 together with the X-ray crystal structures data of RuL2.[10] As a result of the more spatially extended 4d orbital and the large ligand field splitting, in Ru^{II} the three d orbitals are doubly occupied by six d electrons; therefore, Ru^{II} tends to form low-spin pseudo-octahedral coordination. This low-spin arrangement can be obtained from the higher-energy e_g*-like orbital, which will forbid electron transition from the low-energy t_{2g} orbital to the e_g*-like orbital and therefore maintain the low-spin arrangement. The calculated bond angles of N2–Ru–N4 are about 171°, indicating the linear arrangement of the N2, Ru, and N4 atoms. The calculated dihedral angles of N6–N5–Ru–N4 and N1–N2–Ru–N5 are ca. 90°, indicating that the three ligands are almost perpendicular to each other. These calculated geometrical parameters are in general agreement with the X-ray experimental data. For example, the average calculated/experimental Ru–N distance for RuL2 is 2.106/2.058 Å, which is elongated 2.3% by calculation. The largest deviation is 6° for the dihedral angle of N6–N5–Ru–N4 between the calculated and the experimental data. The reason for these differences is that the crystal packing forces in experiment are not considered in the current calculations (performed on single molecule).

Replacement of the pyridine ring in L1 with pyrazine in L2 greatly increased the π-accepting ability of L2. This can be reflected by the shortened Ru–N1 bond length in RuL2 relative to that in RuL1. The strong σ-donor properties of

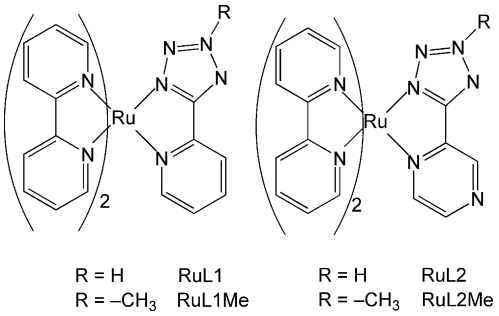

Scheme 1. Sketch structures of the four complexes.

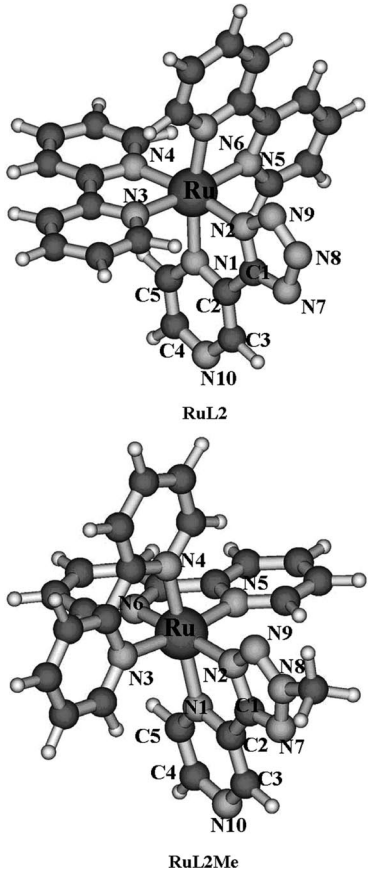

Figure 1. The optimized ground-state geometrical structures for RuL2 and RuL2Me.

the tetrazole, together with the stronger π-accepting ability of the pyrazine fragment,[18] may provide a synergism of the electron delocalization so that the electron density is transferred from tetrazole to the metal ion and back to the pyrazine ride, thus enhancing the chelate interaction. This strengthened interaction between metal and L2 will inevitably cause the slightly relaxed interaction between the metal and bpy moiety, which has donor character. The slightly elongated Ru–N*n*(n = 2–6) in RuL2 can be clearly seen from Table 1. In addition, this weakened interaction between metal and bpy will result in the weakened orbital overlap between the metal and ligands, which will increase the possibility of nonradiative emission in RuL2.

Upon addition of a methyl group to the tetrazolate ring, the interannular π conjugation of the tetrazolate ring significantly enhanced in RuL1Me and RuL2Me compared with that in RuL1 and RuL2. This can be seen from the changes in bond lengths in the tetrazolate ring. For example, the N2–C1, N2–N9, N9–N8, N8–N7, and N7–C1 bonds change from 1.355, 1.333, 1.328, 1.342, and 1.337 Å in RuL1 to 1.366, 1.315, 1.326, 1.328, and 1.331 Å in RuL1Me. This enhanced π conjugation will consequently contract the tetrazolate ring and weaken the interaction between the tetrazolate moiety and the metal. Table 1 shows that almost all the Ru–N bonds in RuL1Me are elongated compared with that in RuL1, and the largest deviation is focused on Ru–N2. These Ru–N bond stretchings in RuL1Me may significantly facilitate the nonradiative decay channels. In RuL2Me, some Ru–N bonds are elongated and some are contracted, which shows an asymmetrical distortion.

To further investigate the bonding interactions, Mulliken population analysis and measured electrochemical data are presented in Table 2. Mulliken population analysis, although not very accurate, will give roughly the major charge transfers and bonding interactions occurring in a molecule.[19] For all cases, the Mulliken atom charge on the Ru atom is about +0.8|e⁻|, which is much less ionic than the formal oxidation state of +2, indicating the considerable donation of electron density into the 4d orbital from the surrounding ligands. It is noted that the Mulliken atom charge on the pyrazine moiety (+0.104|e⁻|) is more negative than that on the pyridine moiety (+0.161|e⁻|), and similarly, a decrease in negative charge on the tetrazole moiety from –0.593|e⁻| in RuL1 to –0.577|e⁻| in RuL2, which indicates an increased π-accepting ability of pyrazine relative to that of pyridine. The methylated complexes RuL1Me and RuL2Me have similar trends to RuL1 and RuL2. As shown in Table 2, the gradually increased positive charge from RuL1 to RuL2Me indicates that the oxidizing ability of the Ru atom in the complexes gradually increases. This is consistent with the measured oxidation potentials in the follow order: 1.03 V (RuL1) < 1.20 V (RuL2) < 1.41 V (RuL1Me) < 1.52 V (RuL2Me). This gradual increase in oxidizing ability of the central Ru atom also indicates the greatly increased π-accepting ability of the ancillary ligands.

Table 2. Mulliken charge on different fragments calculated at the B3LYP level and the experimental half-wave ($-E_{1/2}$) redox potentials.

	Mulliken charge |e⁻|			Redox data[10]	
	Ru	bpy	L	(ox)–$E_{1/2}$ [V]	(red)–$E_{1/2}$ [V]
RuL1	0.793	0.769	–0.432	1.03	–1.40
RuL2	0.800	0.801	–0.473	1.20	–1.39
RuL1Me	0.806	0.625	0.371	1.41	–1.34
RuL2Me	0.813	0.980	0.193	1.52	–1.12

Frontier Molecular Orbital Properties

The frontier molecular orbitals of the ground states (S_0) are very important because they are closely related to the

spectral properties. The frontier molecular orbital compositions of RuL1–RuL2Me are given in Tables S1–S4 (Supporting Information). Energy levels of the orbitals and contour plots of HOMO–LUMO+3 and LUMO+9 are shown in Figure S1 (Supporting Information) and Figure 2, respectively. Tables S1 and S2 (Supporting Information) show that the higher-lying occupied molecular orbitals (MOs) HOMO–HOMO–5 are similar for RuL1 and RuL2. Taking RuL1 as an example, the HOMO lying at –8.22 eV, is dominantly composed of 67.8% d(Ru) (57.8% d_{z^2}), which is antibonding combination with the π orbital of L1 ligand (22.8% in composition). HOMO–1 and HOMO–2 are similar in composition to HOMO, but with slightly different composition of d(Ru). HOMO–3 to HOMO–5 are mainly localized on L1 ligand and have vanishing (HOMO–4, HOMO–5) or very small (HOMO–3) metal character. For unoccupied MOs, ancillary ligands have a more significant affect than that on the occupied MOs. As shown in Figure S1 (Supporting Information), the unoccupied molecular orbitals in RuL2 are lower in energy than the corresponding ones in RuL1. For both complexes, LUMO and LUMO+1 are dominantly localized on the bpy moiety with more than 94% composition. The first L1-based π* orbital exists in LUMO+3 in RuL1, whereas the first L2-based π* orbital exists in LUMO+2 in RuL2. This is due to the greater π-accepting ability of the pyrazine ring, which results in a lower L2-based π* orbital by exchanging the LUMO+2 and LUMO+3 characters.

RuL1Me and RuL2Me are significantly different both in composition distribution and energy levels with respect to RuL1 and RuL2. For RuL1Me (Table S3, Supporting Information), the HOMO is predominantly Ru d orbital (77.7% d_{z^2}) in nature antibonding with only small bpy π orbital (12.5%), but the composition from L1Me ligand vanishes. HOMO–1 and HOMO–2, which are very close in energy within 0.01 eV, are quasidegenerate orbitals mainly contributed by ca. 79% Ru d orbital mixed with some bpy π-orbital composition. HOMO–3 and HOMO–4 are other quasidegenerate orbitals localized on bpy moieties, which is completely different from RuL1 and RuL2. The higher occupied MOs suggest better electron-donating ability, and the lower unoccupied MOs indicate better electron-accepting ability.[20] Figure S1 (Supporting Information) shows that the much lower occupied molecular orbitals of RuL1Me and RuL2Me compared with that in RuL1 and RuL2 indicates that the electron-donating ability of bpy ligands decreases significantly in RuL1Me and RuL2Me, which is consistent with the weakened interaction between the metal Ru atom and the bpy moieties as shown in Table 1. In addition, comparing RuL1Me and RuL2Me with RuL1 and RuL2, the L1Me and L2Me-based π* orbital appears at LUMO+2 and LUMO, respectively, relative to the LUMO+3 and LUMO+2 in RuL1 and RuL2. The much lower unoccupied MOs of RuL1Me and RuL2Me result from the electron-donating character of the CH_3 group, which can transfer electrons from the tetrazol-

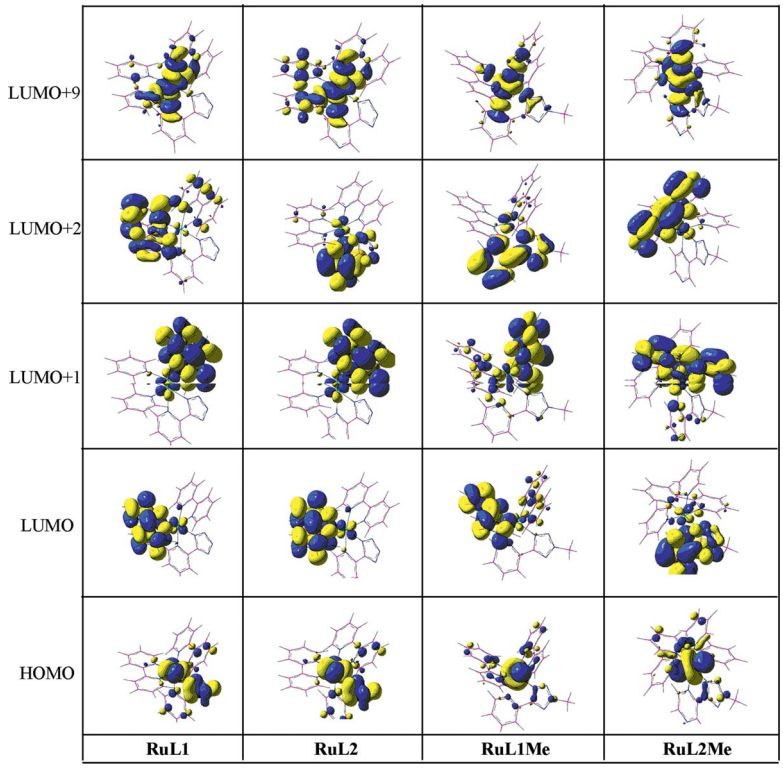

Figure 2. Contour plots of frontier molecular orbitals and e^*_g-like d orbitals of the four complexes in the ground states.

ate moiety to the pyridine or pyrazine moiety and, therefore, greatly stabilize both the occupied and unoccupied orbitals. In addition, Figure 2 shows that the associated e_g*-like orbital is higher in energy, which are recognized as LUMO+9 for these complexes. It is notable that such a large d orbital splitting will not facilitate the electron transition from the t_{2g} orbital to the e_g*-like orbital and, therefore, the low-spin arrangement in the three t_{2g} orbitals is maintained.

Absorption Spectra

TDDFT calculations underestimated the low-energy MLCT and ligand-to-ligand charge-transfer (LLCT) transitions compared with the lowest experimental absorption bands.[16b,21] In our calculations, starting from the ground-state geometries, the lowest 80 singlet–singlet excited states were calculated by the TDDFT/B3LYP method both in the gas phase and in solution. The selected calculated singlet excited states [oscillator strength (f) > 0.04] are listed in Tables 3, 4, 5, and 6 for RuL1–RuL2Me, and the spectra data in the gas phase are listed in Table S5 (Supporting Information). The 10 lowest triplet excited states of the four complexes were also calculated in solution by using the same method and the calculated results are listed in Tables S6–S9 (Supporting Information). The simulated Gaussian-type absorption curves both in the gas phase and in solution with the use of the calculated singlet excited states are listed in Figure 3. To intuitively understand the transition process, the molecular orbital involved in transitions are shown in Figure S1 (Supporting Information) and the lowest-lying absorption transitions are displayed in Figure 4.

In general, all these complexes show a blueshift in the polarized solution compared with those in the gas phase. This is in agreement with the reported experimental data by Che et al.,[22] who pointed out that when the polarity of the solvent increases from benzene to CH_2Cl_2, acetonitrile, and ethanol, the broad low-energy absorption band experi-

Table 3. Selected calculated wavelengths/energies, oscillator strengths (f), major contributions, and transition characters of RuL1 and comparison with experimental data.

States	λ [nm] / E [eV]	f	Major contribution	Character	Expt.[10]
S_1	485/2.55	0.0017	H→L (90%)	MLCT/LLCT	
S_5	423/2.93	0.1380	H–2→L (55%)	MLCT/LLCT/ILCT	
			H–1→L+1 (40%)	MLCT/LLCT/ILCT	
S_6	405/3.06	0.0494	H–1→L+1 (43%)	MLCT/LLCT/ILCT	
			H–2→L (40%)	MLCT/LLCT/ILCT	
S_{10}	346/3.58	0.0467	H–2→L+2 (49%)	MLCT/LLCT/ILCT	
S_{25}	309/4.01	0.0423	H→L+7 (82%)	MLCT/ILCT	
S_{35}	273/4.55	0.0780	H–6→L+1 (32%)	ILCT	
S_{36}	271/4.57	0.1627	H–6→L+1 (49%)	ILCT	
S_{37}	271/4.58	0.3766	H–4→L+1 (38%)	LLCT	
S_{39}	266/4.66	0.4854	H–3→L+2 (68%)	MLCT/LLCT	289
S_{41}	260/4.77	0.0425	H–3→L+3 (94%)	MLCT/ILCT	
S_{57}	236/5.25	0.1320	H–3→L+7 (94%)	MLCT/ILCT	244
S_{63}	229/5.41	0.0494	H–10→L (34%)	LLCT	
S_{64}	229/5.42	0.0461	H–4→L+4 (30%)	LLCT	

Table 4. Selected calculated wavelengths/energies, oscillator strengths (f), major contributions, and transition characters of RuL2 and comparison with experimental data.

States	λ [nm] / E [eV]	f	Major contribution	Character	Expt.[10]
S_1	468/2.65	0.0019	H→L (83%)	MLCT/LLCT	
S_7	407/3.05	0.1049	H–1→L+2 (39%)	MLCT/LLCT/ILCT	
			H–2→L (29%)	MLCT/LLCT/ILCT	
S_8	399/3.11	0.0832	H–2→L (35%)	MLCT/LLCT/ILCT	
			H–1→L+1 (34)	MLCT/LLCT/ILCT	
S_{21}	312/3.98	0.0489	H–1→L+5 (37%)	MLCT/LLCT/ILCT	
S_{31}	289/4.29	0.0763	H–3→L+2 (48%)	MLCT/ILCT	
S_{33}	283/4.38	0.0521	H–2→L+7 (42%)	MLCT/LLCT/ILCT	
S_{37}	275/4.51	0.0477	H–4→L+2 (53%)	MLCT/ILCT	
S_{38}	272/4.56	0.1209	H–5→L+2 (69%)	LLCT	
S_{39}	271/4.58	0.2049	H–4→L+2 (35%)	MLCT/ILCT	
S_{40}	270/4.60	0.0894	H–6→L (58%)	ILCT	
S_{41}	269/4.61	0.0569	H–6→L+1 (72%)	ILCT	
S_{42}	268/4.62	0.3294	H–2→L+10 (28%)	MLCT/LLCT/ILCT	287
S_{43}	267/4.64	0.1517	H–2→L+10 (54%)	MLCT/LLCT/ILCT	
S_{48}	253/4.90	0.0464	H–3→L+3 (96%)	MLCT/LLCT	
S_{52}	243/5.11	0.1769	H–3→L+4 (79%)	MLCT/LLCT	244
S_{73}	225/5.50	0.0546	H–4→L+6 (33%)	MLCT/LLCT	

Table 5. Selected calculated wavelengths/energies, oscillator strengths (*f*), major contributions, and transition characters of RuL1Me and comparison with experimental data.

States	λ [nm] / E [eV]	f	Major contribution	Character	Expt.[10]
S_1	427/2.90	0.0007	H→L (74%)	MLCT/ILCT	
S_6	387/3.21	0.0961	H–1→L (42%)	MLCT/ ILCT	
S_8	377/3.29	0.1209	H–2→L+1 (49%)	MLCT/ ILCT	
			H–2→L+2 (33%)	MLCT/LLCT	
S_{20}	300/4.13	0.0568	H–1→L+7 (62%)	MLCT/ILCT	
S_{27}	291/4.26	0.0580	H–1→L+6 (49%)	MLCT/LLCT	
S_{38}	270/4.59	0.2840	H–4→L+2 (30%)	LLCT	285
S_{39}	267/4.64	0.6268	H–3→L+1 (39%)	ILCT	
S_{42}	248/5.00	0.0512	H–3→L+3 (88%)	LLCT/ILCT	
S_{43}	247/5.03	0.3098	H–5→L+2 (80%)	ILCT	242
S_{46}	236/5.25	0.0476	H–4→L+4 (88%)	LLCT/LLCT	
S_{61}	219/5.65	0.0657	H–2→L+11 (44%)	MLCT/ILCT	

Table 6. Selected calculated wavelengths/energies, oscillator strengths (*f*), major contributions, and transition characters of RuL2Me and comparison with experimental data.

States	λ [nm]/E [eV]	f	Major contribution	Character	Expt.[10]
S_1	459/2.70	0.0012	H→L (97%)	MLCT/LLCT	
S_5	298/3.12	0.1127	H–2→L (90%)	MLCT/LLCT	
S_8	372/3.33	0.1265	H–2→L+21 (28%)	MLCT/ ILCT	
			H–1→L+2 (27%)	MLCT	
S_{22}	301/4.12	0.0638	H–2→L+4 (41%)	MLCT/LLCT/ILCT	
S_{31}	286/4.33	0.0511	H–3→L+1 (25%)	ILCT	
S_{33}	281/4.41	0.0615	H–2→L+6 (39%)	MLCT/LLCT	
S_{38}	268/4.63	0.1542	H–2→L+7 (23%)	MLCT/ ILCT	
S_{39}	267/4.64	0.1829	H–1→L+7 (42%)	MLCT	
S_{41}	265/4.68	0.4522	H–1→L+8 (43%)	MLCT	282
S_{43}	258/4.81	0.3027	H–6→L (56%)	ILCT	242
S_{44}	256/4.84	0.1123	H–4→L+3 (67%)	LLCT/ILCT	
S_{52}	236/5.25	0.0622	H–4→L+5 (86%)	ILCT	
S_{61}	225/5.51	0.0500	H–10→L (53%)	LLCT	
S_{63}	223/5.57	0.0633	H–10→L (39%)	LLCT	
			H–6→L+3 (31%)	LLCT/ILCT	
S_{69}	217/5.71	0.0452	H–7→L+2 (37%)	ILCT	

ences a blueshift. Our previous theoretical calculations also show the same results.[15k] Taking RuL1 as an example, the S_1 absorption bands show a comparatively strong solvent-dependent effect: the 539 nm absorption in the gas phase corresponds to the 485 nm in solution. For other transitions, which are assigned mainly to $\pi \rightarrow \pi^*$ characters, the solvent effect was minor.[23] The calculated results in solution are more in agreement with the experimental values, and therefore, in the later discussion, we will focus on the results in solution.

In experiment, the observed absorption spectra show intense transitions at high energy (200–350 nm) and weaker bands in the visible region (400–500 nm).[10] Obviously, our calculated absorption spectra can well reproduce the experimental features in terms of band positions, intensities and separations. Tables 3–6 show that the lowest energy transitions follow the order RuL1 (485 nm) > RuL2 (468 nm) > RuL2Me (459 nm) > RuL1Me (427 nm), which is consistent with the trend of the energy gap because of the HOMO→LUMO transition (the coefficient in the configuration interaction wave functional is more than 0.70), which contributes mainly to the $S_0 \rightarrow S_1$ electronic absorption. Table S1 (Supporting Information) shows that HOMO of RuL1 is composed of 52.3% d_{z^2} and 22.8% π(L1), whereas LUMO is mainly localized on the bpy ligand with 94.0% composition. Thus, this absorption can be assigned as the $\{[d_{z^2}\ (Ru) + \pi(L1)] \rightarrow [\pi^*(bpy)]\}$ transition with character of MLLCT (metal–ligand to ligand charge transfer). The 468 nm absorption of RuL2 has similar character to RuL1, but with different composition of d orbital, whereas for RuL1Me the MLCT $[d_{z^2}\ (Ru) \rightarrow \pi^*(bpy)]$ is the main transition mixed with a small intraligand $\pi \rightarrow \pi^*$ $[\pi(bpy) \rightarrow \pi^*(bpy)]$ contribution. In addition to the MLCT, the LLCT character $[\pi(bpy) \rightarrow \pi^*(L2Me)]$ also contributes to the 459 nm absorption of RuL2Me. As a result of the negligible intensity (f = 0.0007–0.0019), these $S_0 \rightarrow S_1$ transitions are more probably forbidden and would be practically absent in the absorption spectra.

For RuL1 and RuL2, the experimental observed first distinguishable absorption at 468 and 432 nm and at 447 and 429 nm may correspond to the calculated triplet transitions as listed in Tables S6 and S7 (Supporting Information), and some absorption bands are composed of a series of transitions. Similarly, the 430 and 410 nm bands in RuL1Me and RuL2Me may also contributed by the singlet → triplet transitions due to the strong spin–orbit coupling. As expected, the computed triplet states fall in a smaller energy range than the calculated singlet states.

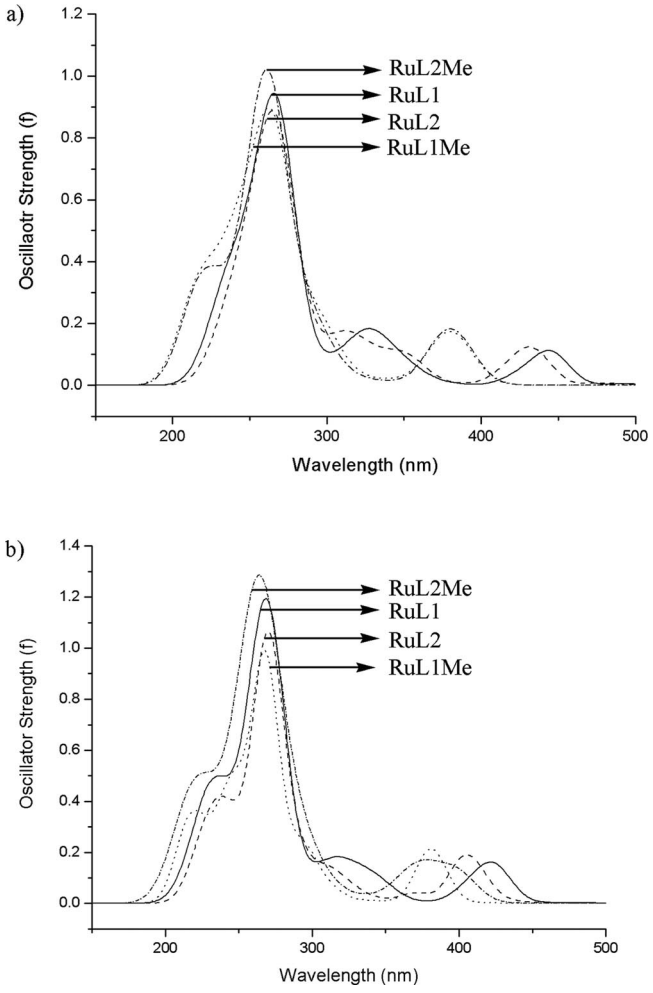

Figure 3. The simulated singlet absorption spectra in the gas phase (a) and in acetonitrile solvent (b) of the four complexes.

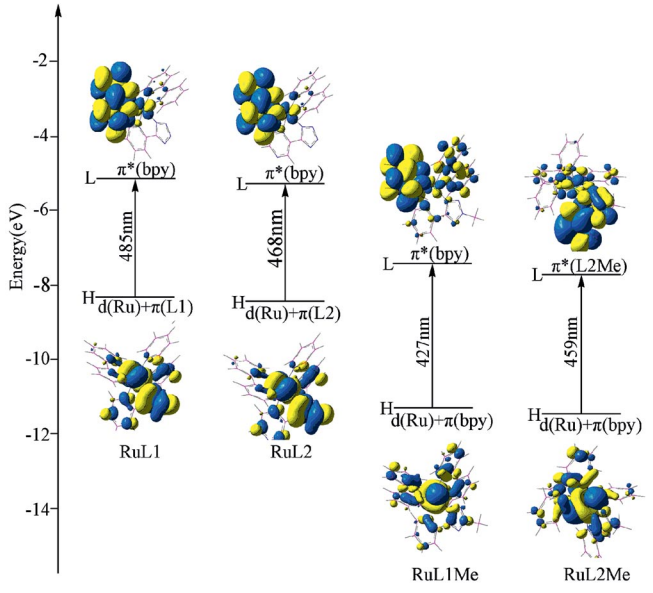

Figure 4. Transitions responsible for the lowest-lying absorptions at 485, 468, 427, and 459 nm for RuL1, RuL2, RuL1Me, and RuL2Me, respectively.

The experimentally observed strongest absorptions around 280 nm are mainly assigned as ligand-centered bpy-based $\pi \rightarrow \pi^*$ absorptions.[10] In our calculations, these absorption peaks are blueshifted to a higher energy region, and all the bands arise from a combination of several transitions, among which only those having the major contribution are listed in Tables 3–6. The observed absorption band at 289 nm for RuL1 is mainly described by a series of very close transitions (271, 270, and 266 nm) and they are assigned to {[d(Ru) + π(L1 + bpy)] → [π*(bpy)]} with character of MLLCT and ILCT. The absorption band observed at 287 nm for RuL2 is calculated at 272, 271, 268, and 267 nm, and can be assigned to LLCT [π(L2) → π*(bpy)] transition perturbed small MLCT contribution. For RuL1Me, the calculated 270 and 267 nm absorptions contribute to the 285 nm band and can mainly be characterized by LLCT and ILCT transitions, in which an electron promoted from the bpy-based π orbital to the L1Me and bpy-based π* orbital. RuL2Me has a similar transition character to RuL2, such as MLCT, LLCT, and ILCT. The observed higher-energy absorptions at around 240 nm are mainly contributed by intra/interligand absorption (Tables 3–6). This slightly larger deviation between the calculated and the experimental absorption in the higher energy region relative to the lower energy region is a general trend already observed in many Ru^{II}–polypyridyl complexes.[23a,23b] These studies show that the low energy MLCT transitions were described satisfactorily with rather small basis sets, whereas higher energy $\pi \rightarrow \pi^*$ transitions needed higher quality basis sets.

The calculated results agree with the experimental observations[10] that the MLCT component is more remarkable in the lower energy region. The above calculation indicates that spin-selection rules are not strictly obeyed for heavy metal complexes and the singlet-to-triplet transitions are facilitated by the enhanced spin–orbit coupling in heavy atom. The non-negligible MLCT participating in the lower energy region is an indicator for efficient intersystem crossing, and the dipole-allowed singlet–triplet transitions ensure the high luminescence efficiency of ruthenium(II) polypyridine complexes, especially for RuL2Me, which elucidates their higher quantum yields relative to those of RuL1 and RuL2.

Efficiency Comparison

From experimental results, we know that complexes with different ancillary ligands show significant diversity in photophysical properties, from the poorly emissive RuL2 to the stronger radiative decay of RuL2Me. From the experimental data, we obtained the k_r (radiative decay rate) and k_{nr} (nonradiative decay rate) values, $k_r = \Phi/\tau$ and $k_{nr} = (1-\Phi)/\tau$, where τ is the lifetime and Φ is the quantum yield. Obviously, Φ can be affected by the competition between k_r and k_{nr}, namely, $\Phi = k_r/(k_r + k_{nr})$. Therefore, to increase the quantum yield, k_r should be increased and k_{nr} should be decreased simultaneously or respectively.[24] Our calculated

k_r and k_{nr} data are listed in Table 7. The k_r value of RuL1 is about three times smaller than that of RuL2, and the larger k_r value of RuL2 is due to the larger metal-based Ru d orbital composition in HOMO than that in RuL1. The HOMO-to-LUMO transition contributes mainly to the lowest-energy emission, because the energy gaps between HOMO and HOMO–1, LUMO and LUMO+1 are larger and these large energy gaps may demonstrate the difficulty of the electronic transition from HOMO–1 or lower occupied MOs to LUMO+1 or higher unoccupied MOs. The larger d orbital composition can result in the larger ^{3}MLCT participation in emission process and quantum efficiencies could be increased by larger ^{3}MLCT composition.[25] De Angelis and Chi el at.[26] concluded that intersystem crossing could be enhanced by notable ^{3}MLCT participation, namely, the phosphorescence in which $^3\pi\pi^*$ mixed with ^{3}MLCT excited state should be greatly increased by increasing the ratio of ^{3}MLCT: $^3\pi\pi^*$. The largest k_r value in RuL2Me is due to the same reason to RuL2, whereas in RuL1Me, the k_r value is lower than others though it has a higher metal-based d orbital composition. This may be due to the general Ru–N stretching relative to the other three, which will decrease the metal–ligand bonding strengths due to the antibonding character, accompanied by stabilizing the metal-centered (MC) excited state, and consequently the reduction of the radiative deactivation.[27] This can be evidenced by the energy difference between the ^{1}MC state and the lowest-lying ^{1}MLCT state, 2.48 eV for RuL1, 2.43 eV for RuL2, 2.03 eV for RuL1Me, and 2.10 eV for RuL2Me.

Table 7. The calculated radiative decay rate (k_r) and nonradiative decay rate (k_{nr}), together with the measured lifetime (τ) and quantum yields (Φ).

	k_r [$\times 10^5$ s^{-1}]	k_{nr} [$\times 10^5$ s^{-1}]	τ[10] [ns]	Φ[10] [$\times 10^{-3}$]
RuL1	1.8	4.5	220	4
RuL2	5.0	170	6	0.3
RuL1Me	0.12	1.2	826 (160)	1
RuL2Me	26.0	1.2	820	21

For k_{nr} values, RuL2 has the largest value among these complexes. This is a result of the fact that the other effects of vibrational relaxation, quenching and energy transfer, intersystem crossing (ISC), internal conversion (IC), and interaction with the solvent molecules can prevent the system from undergoing radiative decay emission pathways. The calculated dipole moments of RuL1, RuL2, RuL1Me, and RuL2Me are 12.02, 13.29, 0.36, and 3.41 D, respectively, and the larger dipole moments indicate the larger polarity. The larger k_{nr} values in RuL1 and RuL2 are due to the fact that the effect of solvent CH_3CN on RuL1 and RuL2 is larger than on RuL1Me and RuL2Me due to their stronger polarity. Therefore, RuL1 and RuL2 can more easily convey the excited-state energy to the polar solvent towards the nonradiative decay pathways. Furthermore, the electron-deficient pyrazole ring plays a crucial role as an electron acceptor in the charge-transfer process, because the CN^- group in solvent has electron-donating nature, which can further accelerate the energy conveying process in RuL2 and results in the shortest lifetime and largest k_{nr} value in RuL2. For RuL1Me and RuL2Me, the molecule polarity is much smaller than RuL1 and RuL2 as a result of their smaller dipole moments and, therefore, the interaction between CH_3CN solvent and RuL1Me and RuL2Me is weaker. Furthermore, the attached CH_3 group is a good electron-donating group, which can to a large extent prevent or buffer the polarity–polarity interaction between the solvent molecules and RuL1Me and RuL2Me as a result of the presence of intramolecular charge transfer, which prevents energy conveyance to the surrounding solvent. Therefore, the energy loss to polar solvent in RuL1Me and RuL2Me is much reduced and they have rather longer radiative lifetimes and nearly the same and smaller k_{nr} values. Of course, other factors, such as temperature,[28] different polarities of solvent,[29] different ligand bite angles,[30] and vibrational decay[31] can all influence the lifetime and quantum yield of transition-metal complexes to different extents. Because the four complexes studied in this paper were measured under the same experimental conditions and have similar ligand frameworks, these other factors are negligible. The trade-off between the k_r and k_{nr} values and the large decline in the quantum efficiency in RuL2 compared with RuL1 and RuL1Me are due to the greatly increased nonradiative decay, relative to the increased k_r value. The simultaneous increase in k_r and decrease in k_{nr} values result in the highest quantum efficiency in RuL2Me. Therefore, efforts to choose solvents with lower polarity will be rewarded by increases in the quantum yields and phosphorescence efficiency.

Conclusions

In this paper, we reported the investigation of geometries, electronic structures, absorption properties, and phosphorescence efficiency of four $[Ru(bpy)_2L]^+$ complexes, as well as their methylated complexes (RuL1Me and RuL2Me). The calculated results reveal that replacement of the pyridine ring with a pyrazine ring results in better π-accepting ability of L2, which results in a greatly shortened Ru–N1 bond in RuL2 relative to that in RuL1 and a more-negative Mulliken atom charge on pyrazine than on pyridine. Through attaching a CH_3 group on the tetrazolate ring, the π-accepting ability of L1Me and L2Me are further enhanced in RuL1Me and RuL2Me compared with that in RuL1 and RuL2. Different ligands have a more significant effect on the unoccupied molecular orbital composition compared with the influence on occupied molecular orbitals. The enhanced π-accepting ability makes the ^{1}-based π* orbital shift from LUMO+3 in RuL1 to LUMO in RuL2Me. The lowest-energy absorptions are mainly MLCT, LLCT, and/or ILCT in nature, and the MLCT component is more remarkable in the lower energy region in RuL1Me and RuL2Me. Moreover, the lowest quantum yield in RuL2 is due to its larger polarity compared with the other complexes, which allows it to more easily convey the excited-state energy to the polar solvent through nonra-

diative pathways. The electron-donating CH_3 group can prevent or buffer this nonradiative process in RuL2Me and give a smaller k_{nr} value. The increased k_r value is due to increased MLCT participation, and both positive factors result in the highest quantum yields in RuL2Me.

Supporting Information (see footnote on the first page of this article): Calculated frontier molecular orbitals compositions of RuL1–RuL2Me; absorptions of complexes RuL1–RuL2Me calculated by using the TDDFT method in the gas phase; singlet → triplet absorptions of RuL1–RuL2Me in solution.

Acknowledgments

The authors are grateful for financial aid from the National Natural Science Foundation of China (Grant Nos. 20490210, 20631040, 20602035, and 20771099) and the MOST of China (Grant Nos. 2006CB601103 and 2006DFA42610).

[1] J. P. Paris, W. W. Brandt, *J. Am. Chem. Soc.* **1959**, *81*, 5001–5002.
[2] a) H. Nagashima, H. Kondo, T. Hayashida, Y. Yamaguchi, M. Gondo, S. Masuda, K. Miyazaki, K. Matsubara, K. Kirchner, *Coord. Chem. Rev.* **2003**, *245*, 177–190; b) P. D. Beer, E. J. Hayes, *Coord. Chem. Rev.* **2003**, *240*, 167–189.
[3] V. Balzani, G. Bergamini, F. Marchioni, P. Ceroni, *Coord. Chem. Rev.* **2006**, *250*, 1254–1266.
[4] a) F. Szemes, D. Hesek, Z. Chen, S. W. Dent, M. G. B. Drew, A. J. Goulden, A. R. Graydon, A. Grieve, R. J. Mortimer, T. Wear, J. S. Weightman, P. D. Beer, *Inorg. Chem.* **1996**, *35*, 5868–5879; b) M. S. Vickers, K. S. Martindale, P. D. Beer, *J. Mater. Chem.* **2005**, *15*, 2784–2790.
[5] a) M. Grätzel, *Coord. Chem. Rev.* **1991**, *111*, 167–174; b) M. K. Nazeeruddin, C. Klein, P. Liska, M. Grätzel, *Coord. Chem. Rev.* **2005**, *249*, 1460–1467.
[6] A. Juris, V. Balzani, F. Barigelletti, S. Campagna, P. Belser, A. Zelewsky, *Coord. Chem. Rev.* **1988**, *84*, 185–277.
[7] a) G. R. Newkome, A. K. Patri, E. Holder, U. S. Schubert, *Eur. J. Org. Chem.* **2004**, 235–254; b) C. J. Elsevier, J. Reedijk, P. H. Walton, M. D. Ward, *Dalton Trans.* **2003**, 1869–1880; c) V. Balzani, A. Juris, M. V. Campagna, S. Serroni, *Chem. Rev.* **1996**, *96*, 759–834; d) E. A. Medlycott, G. S. Hanan, *Chem. Soc. Rev.* **2005**, *34*, 133–142.
[8] a) M. Haga, T. Takasugi, A. Tomie, M. Ishizuya, T. Yamada, M. D. Hossain, M. Inoue, *Dalton Trans.* **2003**, 2069–2079; b) M. J. Han, L. H. Gao, Y. Y. Lü, K. Z. Wang, *J. Phys. Chem. B* **2006**, *110*, 2364–2371.
[9] a) A. C. Benniston, A. Harriman, P. Y. Li, C. A. Sams, *J. Am. Chem. Soc.* **2005**, *127*, 2553–2564; b) A. Barbieri, B. Ventura, F. Barigelletti, A. D. Nicola, M. Quesada, R. Ziessel, *Inorg. Chem.* **2004**, *43*, 7359–7368.
[10] S. Stagni, E. Orselli, A. Palazzi, L. D. Cola, S. Zacchini, C. Femoni, M. Marcaccio, F. Paolucci, S. Zanarini, *Inorg. Chem.* **2007**, *46*, 9126–9138.
[11] P. Hohenberg, W. Kohn, *Phys. Rev.* **1964**, *136*, B864–B871.
[12] a) C. Lee, W. T. Yang, R. G. Parr, *Phys. Rev. B* **1988**, *37*, 785–789; b) A. D. Becke, *J. Chem. Phys.* **1993**, *98*, 5648–5662.
[13] a) J. Autschbach, T. Ziegler, S. J. A. Gisbergen, E. J. Baerends, *J. Chem. Phys.* **2002**, *116*, 6930–6940; b) T. Helgaker, P. Jørgensen, *J. Chem. Phys.* **1991**, *95*, 2595–2601; c) K. L. Bak, P. Jørgensen, T. Helgaker, K. Rund, H. J. A. Jensen, *J. Chem. Phys.* **1993**, *98*, 8873–8887.
[14] B. Mennucci, J. Tomasi, *J. Chem. Phys.* **1997**, *106*, 5151–5158.
[15] a) R. A. Kirgan, D. P. Rillema, *J. Phys. Chem. A* **2007**, *111*, 13157–13162; b) J. M. Villegas, S. R. Stoyanov, W. Huang, D. P. Rillema, *Inorg. Chem.* **2005**, *44*, 2297–2309; c) S. Fantacci, F. De Angelis, A. Selloni, *J. Am. Chem. Soc.* **2003**, *125*, 4381–4387; d) D. D. Censo, S. Fantacci, F. De Angelis, C. Klein, N. Evans, K. Kalyanasundaram, H. J. Bolink, M. Grätzel, M. K. Nazeeruddin, *Inorg. Chem.* **2008**, *47*, 980–989; e) M. K. Nazeeruddin, F. De Angelis, S. Fantacci, A. Selloni, G. Viscardi, P. Liska, S. Ito, B. Takeru, M. Grätzel, *J. Am. Chem. Soc.* **2005**, *127*, 16835–16847; f) C. Barolo, M. K. Nazeeruddin, S. Fantacci, D. D. Censo, P. Comte, P. Liska, G. Viscardi, P. Quagliotto, F. De Angelis, M. Grätzel, *Inorg. Chem.* **2006**, *45*, 4642–4653; g) L. L. Shi, Y. Liao, L. Zhao, Z. M. Su, Y. H. Kan, G. C. Yang, S. Y. Yang, *J. Organomet. Chem.* **2007**, *692*, 5368–5374; h) I. V. Novozhilova, A. V. Volkov, P. Coppens, *Inorg. Chem.* **2004**, *43*, 2299–2307; i) I. V. Novozhilova, A. V. Volkov, P. Coppens, *Inorg. Chem.* **2004**, *43*, 2299–2307; j) X. N. Li, X. J. Liu, Z. J. Wu, H. J. Zhang, *J. Phys. Chem. A* **2008**, *112*, 11190–11197; k) X. N. Li, J. K. Feng, A. M. Ren, L. J. Li, *Synth. Met.* **2007**, *157*, 1046–1053; l) X. N. Li, J. K. Feng, A. M. Ren, *Chin. J. Chem.* **2008**, *26*, 1979–1984.
[16] a) P. J. Hay, W. R. Wadt, *J. Chem. Phys.* **1985**, *82*, 270–283; b) P. J. Hay, W. R. Wadt, *J. Chem. Phys.* **1985**, *82*, 299–310.
[17] M. J. Frisch, G. W. Trucks, H. B. Schlegel, G. E. Scuseria, M. A. Robb, J. R. Cheeseman, J. A. Montgomery Jr., T. Vreven, K. N. Kudin, J. C. Burant, J. M. Millam, S. S. Iyengar, J. Tomasi, V. Barone, B. Mennucci, M. Cossi, G. Scalmani, N. Rega, G. A. Petersson, H. Nakatsuji, M. Hada, M. Ehara, K. Toyota, R. Fukuda, J. Hasegawa, M. Ishida, T. Nakajima, Y. Honda, O. Kitao, H. Nakai, M. Klene, X. Li, J. E. Knox, H. P. Hratchian, J. B. Cross, C. Adamo, J. Jaramillo, R. Gomperts, R. E. Stratmann, O. Yazyev, A. J. Austin, R. Cammi, C. Pomelli, J. W. Ochterski, P. Y. Ayala, K. Morokuma, G. A. Voth, P. Salvador, J. J. Dannenberg, V. G. Zakrzewski, S. Dapprich, A. D. Daniels, M. C. Strain, O. Farkas, D. K. Malick, A. D. Rabuck, K. Raghavachari, J. B. Foresman, J. V. Ortiz, Q. Cui, A. G. Baboul, S. Clifford, J. Cioslowski, B. B. Stefanov, G. Liu, A. Liashenko, P. Piskorz, I. Komaromi, R. L. Martin, D. J. Fox, T. Keith, M. A. Al-Laham, C. Y. Peng, A. Nanayakkara, M. Challacombe, P. M. W. Gill, B. Johnson, W. Chen, M. W. Wong, C. Gonzalez, J. A. Pople, *Gaussian 03*, Revision D.01, Gaussian, Inc., Wallingford, CT, **2004**.
[18] R. Hage, J. G. Haasnoot, J. Reedijk, R. Y. Wang, J. G. Vos, *Inorg. Chem.* **1991**, *30*, 3263–3269.
[19] D. Q. Wang, C. Y. Zhao, D. L. Phillips, *Organometallics* **2004**, *23*, 1953–1960.
[20] L. C. Xu, J. Li, Y. Shen, K. C. Zheng, L. N. Ji, *J. Phys. Chem. A* **2007**, *111*, 273–280.
[21] a) J. F. Guillemoles, V. Barone, L. Joubert, C. Adamo, *J. Phys. Chem. A* **2002**, *106*, 11354–11360; b) M. Polson, M. Ravaglia, S. Fracasso, M. Garavelli, F. Scandola, *Inorg. Chem.* **2005**, *44*, 1282–1289.
[22] W. Lu, B. X. Mi, M. C. W. Chan, Z. Hui, C. M. Che, N. Y. Zhu, S. T. Lee, *J. Am. Chem. Soc.* **2004**, *126*, 4958–4971.
[23] a) F. De Angelis, S. Fantacci, A. Selloni, *Chem. Phys. Lett.* **2004**, *389*, 204–208; b) S. Fantacci, F. D. Angelis, A. Sgamellotti, N. Re, *Chem. Phys. Lett.* **2004**, *396*, 43–48; c) X. Y. Hu, X. J. Liu, J. K. Feng, *Chin. J. Chem.* **2007**, *25*, 1370–1378.
[24] a) S. Fantacci, F. De Angelis, A. Sgamellotti, A. Marrone, N. Re, *J. Am. Chem. Soc.* **2005**, *127*, 14144–14145; b) A. B. Tamayo, S. Garon, T. Sajoto, P. I. Djurovich, I. M. Tsyba, R. Bau, M. E. Thompson, *Inorg. Chem.* **2005**, *44*, 8723–8732.
[25] M. Abrahamsson, L. Hammarström, D. A. Tocher, S. Nag, D. Datta, *Inorg. Chem.* **2006**, *45*, 9580–9586.
[26] a) P. T. Chou, Y. Chi, *Chem. Eur. J.* **2007**, *13*, 380–395; b) E. Y. Li, Y. M. Cheng, C. C. Hsu, P. T. Chou, G. H. Lee, I. H. Lin, Y. Chi, C. S. Liu, *Inorg. Chem.* **2006**, *45*, 8041–8051; c) Y. Chi, P. T. Chou, *Chem. Soc. Rev.* **2007**, *36*, 1421–1431.
[27] a) A. Vogler, H. Kunkely, *Top. Curr. Chem.* **2001**, *213*, 143–182; b) M. M. Glezen, A. J. Lees, *J. Am. Chem. Soc.* **1988**, *110*, 3892–3897.
[28] J. M. Williams, H. H. Wang, M. A. Beno, T. J. Emge, L. M. Sowa, P. T. Copps, F. Behroozi, L. N. Hall, K. D. Carlson, G. W. Crabtree, *Inorg. Chem.* **1984**, *23*, 3841–3842.

[29] D. L. Rochester, S. Develay, S. Záliš, J. A. G. Williams, *Dalton Trans.* **2009**, 1728–1741.
[30] a) M. Abrahamsson, H. C. Becker, L. Hammarström, C. Bonnefous, C. Chamchoumis, R. P. Thummel, *Inorg. Chem.* **2007**, *46*, 10354–10364; b) M. Abrahamsson, H. Wolpher, O. Johansson, J. Larsson, M. Kritikos, L. Eriksson, P. O. Norrby, J. Bergquist, L. Sun, B. Åkermark, L. Hammarström, *Inorg. Chem.* **2005**, *44*, 3215–3225; c) L. Salassa, C. Garino, G. Salassa, R. Gobetto, C. Nervi, *J. Am. Chem. Soc.* **2008**, *130*, 9590–9597; d) M. Abrahamsson, M. Jäger, T. Österman, L. Eriksson, P. Persson, H. C. Becker, O. Johansson, L. Hammarström, *J. Am. Chem. Soc.* **2006**, *128*, 12616–12617.
[31] R. E. Harding, S. C. Lo, P. L. Burn, I. D. W. Samuel, *Org. Electron.* **2008**, *9*, 377–384.

Received: April 16, 2009
Published Online: August 12, 2009

